

Article

Biochar from Spent Malt Rootlets and Its Application to an Energy Conversion and Storage Device

John Vakros ^{1,*}, Ioannis D. Manariotis ², Vassilios Dracopoulos ³, Dionissios Mantzavinos ¹ and Panagiotis Lianos ^{1,*}

¹ Department of Chemical Engineering, University of Patras, 26500 Patras, Greece; mantzavinos@chemeng.upatras.gr

² Department of Civil Engineering, University of Patras, 26500 Patras, Greece; idman@upatras.gr

³ FORTH/ICE-HT, P.O. Box 1414, 26504 Patras, Greece; indy@iceht.forth.gr

* Correspondence: vakros@chemistry.upatras.gr (J.V.); lianos@upatras.gr (P.L.)

Abstract: Activated carbon obtained from biomass wastes was presently studied in order to evaluate its applicability in an energy storage device. Biochar was obtained by the carbonization of spent malt rootlets and was further processed by mild treatment in NaOH. The final product had a specific surface of 362 m² g⁻¹ and carried Na, P and a few mineral sites. This material was first characterized by several techniques. Then it was used to make a supercapacitor electrode, which reached a specific capacitance of 156 F g⁻¹. The supercapacitor electrode was combined with a photocatalytic fuel cell, making a simple three-electrode device functioning with a single alkaline electrolyte. This device allows solar energy conversion and storage at the same time, promoting the use of biomass wastes for energy applications.

Keywords: biochar; spent malt rootlets; photocatalytic fuel cell; supercapacitors



Citation: Vakros, J.; Manariotis, I.D.; Dracopoulos, V.; Mantzavinos, D.; Lianos, P. Biochar from Spent Malt Rootlets and Its Application to an Energy Conversion and Storage Device. *Chemosensors* **2021**, *9*, 57. <https://doi.org/10.3390/chemosensors9030057>

Academic Editor: Chung-Wei Kung

Received: 9 February 2021

Accepted: 19 March 2021

Published: 22 March 2021

Publisher's Note: MDPI stays neutral with regard to jurisdictional claims in published maps and institutional affiliations.



Copyright: © 2021 by the authors. Licensee MDPI, Basel, Switzerland. This article is an open access article distributed under the terms and conditions of the Creative Commons Attribution (CC BY) license (<https://creativecommons.org/licenses/by/4.0/>).

1. Introduction

Biomass-derived porous carbon materials are enjoying increasing popularity due to their several and very important applications. Porous carbon obtained by the carbonization of biomass is known as “biochar.” Biochar is produced by the pyrolysis of a biomass under an inert atmosphere and it can be further processed by several techniques that increase its porosity and improve its functionality [1]. Biochar carries many advantages: it can be produced from any kind of biomass, is inexpensive and is environmentally friendly. It is estimated that because biochar stores carbon, it reduces CO₂ emissions by 0.1–0.3 billions of tons annually [2]. Biochar can be used as a soil remediation agent [3], as a fuel for energy production and for greenhouse gas reduction, etc. [4]. Biochar has been used as an absorber to retain harmful contaminants [5], as a catalyst in the transesterification of lipids for biodiesel production [6], as catalyst support in various processes [7–9], as an activator of persulfates in advanced oxidation processes [10], as a platform for sensing applications [11] and as supercapacitor for energy storage [1]. These interesting and high-value applications are related to and depend on biochar composition and structural characteristics. In this respect, and as a function of biomass origin and post-pyrolysis treatment, biochar may carry a significant amount of minerals while oxygen, nitrogen and sulfur are chemical agents found in biochar and are responsible for its properties [1]. This broad basis of factors affecting biochar properties increases its popularity and introduces resourceful ideas concerning biomass origin and biochar production processes [12–18]. The present work focuses on the use of biochar as supercapacitor. Indeed, porous carbon, including biochar, makes a very useful and inexpensive material for electronic, in particular supercapacitor, applications [1,19–25].

Supercapacitors are capacitors of very high capacity. The most common category of supercapacitors, which is also related to biomass-derived porous carbons, is the so-called

electrochemical double-layer capacitors [1]. Such capacitors are formed at the interface between an electrode and an electrolyte. When the electrode is charged, ions from the electrolyte are electrostatically attracted at the interface to provide an electric balance. The extent then of energy (charge) storage is obviously related to the active surface of the interface. This is why porous carbons, which may reach specific surface areas of approximately $1000 \text{ m}^2 \text{ g}^{-1}$, provide such high specific surfaces and, being satisfactorily conductive, make proper material for the construction of electrochemical double-layer supercapacitors. In line with the above Introduction, the present work concerns the employment of biochar for the construction and application of a supercapacitor. Although activated carbons have been widely used for energy storage, the use of raw biochar is rather limited. In almost all the studies an activation process is used, commonly with impregnation with KOH and pyrolysis. The application of these materials results in supercapacitors with a specific capacitance of between 74 and 386 F g^{-1} [25–30]. The values are lower in the case of alkaline electrolyte. These studies point out the importance of the high specific area and the presence of a hierarchical pore structure.

The specific goal of this work is to use a material that is readily disposed, namely malt spent rootlets from beer factories, to make a useful product and combine it with a solar energy conversion device in order to make a simple system capable of energy conversion and storage. Biochar powder was produced by malt spent rootlets carbonization, and this powder was used to make a supercapacitor electrode. As a light conversion device we have used a photocatalytic fuel cell [25], i.e., a photoelectrochemical cell that functions by the photocatalytic degradation of an organic fuel, which may be an organic waste. Such a cell is composed of two electrodes: a photoanode electrode carrying a photocatalyst and a cathode electrode, which (usually) functions by atmospheric oxygen reduction. The cell also contains a supporting electrolyte where the fuel is dissolved. If the supercapacitor electrode is added to the photocatalytic fuel cell, it may store charges by forming an electrochemical double layer with the ions of the supporting electrolyte of the cell (see Figure 1). This possibility has been presently studied and the results were very satisfactory.

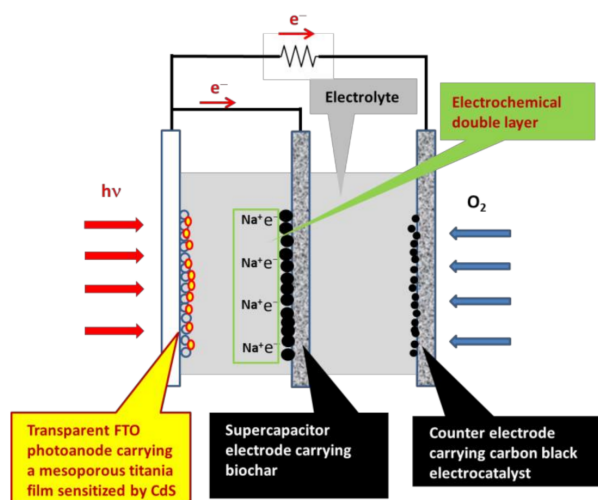


Figure 1. Schematic illustration of the photocatalytic fuel cell carrying a third (supercapacitor) electrode. The photoanode was made by depositing a mesoporous CdS/TiO₂ film on a transparent fluorine doped tin oxide (FTO) electrode. The cathode electrode was a carbon cloth carrying a hydrophobic gas diffusion layer made of carbon black. The supercapacitor electrode was a carbon cloth carrying a film made of biochar particles and a small percentage of carbon black. Photogenerated holes are consumed mainly by oxidation of an added organic fuel and secondarily water. Photogenerated electrons produce an electric current and are partly consumed to charge the supercapacitor. The rest are consumed by reducing atmospheric oxygen.

In a previous work [25], it was found that the application of biochar as a supercapacitor can be competitive with activated carbon. The valorization of raw biomass is an advantage since its processing is considered greener. As noted previously, a good biochar candidate for supercapacitor application should have a high surface area, a balanced distribution of micropores and meso/macro pores and a significant amount of active surface groups. From this perspective, in this work we have studied the application of biochar from spent malt rootlets. In a recent review [31], the applications of spent malt rootlets have been reported. Among other applications, biochar from spent malt rootlets exhibits interesting properties such as great adsorption capacity and high concentration of surface groups. On the other hand, the main disadvantage of raw biochar is the moderate surface area and the high quantity of minerals left after pyrolysis. To reduce this disadvantage, biochar may be modified by treatment, for example, with NaOH, which increases the basicity of the sample and regulates its specific surface area. The treatment with NaOH removes part of the organic phase, especially lignin, and dissolves a significant amount of the minerals [32]. In the present case, biochar obtained from spent malt rootlets has indeed been subjected to a mild treatment with NaOH; therefore, its specific surface area increased, in particular by the extraction of organics, while its surface was enriched with more basic sites. These changes are promising for the application of this biochar as supercapacitor.

2. Materials and Methods

2.1. Biochar Preparation

Raw biochar was prepared by the pyrolysis of spent malt rootlets, one of the main by-products of the brewing industry. The rootlets were provided by the Athenian Brewery S.A., (Patras, Greece). First, the rootlets were dried overnight at 50 °C and sieved into 1.18–0.15 mm. Then, a weighted quantity was placed into custom-made quartz vessels and heated to 900 °C in a gradient temperature furnace (LH 60/12, Nabertherm GmbH, Lilienthal, Germany). The biochar prepared was collected and treated with 1 M NaOH solution under reflux (105 °C) for 30 min. Then, the suspension was cooled to room temperature, filtrated, washed with 1 L of 3D H₂O several times and dried at 120 °C for 2 h. The thus prepared sample, abbreviated Na-BC, was used without further treatment.

2.2. Biochar Characterization

The Na-BC was characterized with various physicochemical techniques. The specific surface area (SSA), the micropores surface area and the pore size distribution of the samples were determined from nitrogen isotherms at −196 °C using a Tristar 3000 Micromeritics instrument. The morphology of the biochar was examined using a scanning electron microscope (SEM) (FEI Quanta 250 FEG) working under different pressures (10–4000 Pa). Energy dispersive spectrometry (EDX) was performed using a scanning electron microscope (SEM)JEOL JSM6300 equipped with an EDX. Fourier transform infrared (FTIR) spectra were recorded on a Perkin Elmer Spectrum RX FTIR spectrometer in the region 4000–400 cm^{−1}. The samples were prepared as KBr pellets with 1% wt/wt biochar. X-ray diffraction (XRD) patterns were recorded in a Bruker D8 Advance diffractometer equipped with a nickel-filtered CuKα (1.5418 Å) radiation. Thermogravimetric analysis (TGA) was performed in a TGA Perkin Elmer system under air atmosphere. Acid-base behavior and the determination of the point of zero charge of the sample was performed with the potentiometric mass titration (PMT) method [33], using a TIM 800 Radiometer Copenhagen Autoburette System equipped with the Timtalk 8, version 2.0 software. More details about the experimental component can be found in the literature [34].

2.3. Construction of the Electrodes

A slurry was made with biochar and it was deposited on a carbon cloth in order to make the supercapacitor electrode. Carbon cloth was cut in the appropriate dimensions providing an active area of 1 cm². The slurry was made by vigorously mixing 8 mL of water, 0.24 g of biochar, 0.06 g of carbon black and 0.1 g of Nafion perfluorinated resin solution

binder. Then the paste was dropped on the carbon cloth and was annealed at 340 °C. The quantity of biochar on the dried electrode was approximately 5 mg. The photoanode electrode was made by depositing a combined CdS/TiO₂ photocatalyst on a transparent fluorine doped tin oxide (FTO) electrode. Details of the photoanode construction have been repeatedly published in the past and they are presently provided in the Supplementary Information File. The counter electrode was made by depositing pure carbon black on carbon cloth without biochar. The components then were 8 mL of water, 0.3 g of carbon black and 0.1 g of Nafion perfluorinated resin.

2.4. Apparatus for Photoelectrochemical Measurements

The photoelectrochemical cell was made of plexiglass and comprised 3 electrodes as schematically shown in Figure 1. A left-side window was sealed by the photoanode electrode. Light reached the photocatalyst through the transparent FTO electrode. A right-side window was sealed by the air cathode electrode (counter electrode). The photoanode and counter electrode were connected by an external circuit, through a potentiostat. The supercapacitor electrode was placed between the anode and the counter electrode and it was short-circuited with the photoanode electrode. The reactor was filled with an electrolyte containing 0.5 M NaOH in which 5% *v/v* ethanol was dissolved. The cell functioned as a photocatalytic fuel cell with ethanol playing the role of fuel. Current-voltage measurements were carried out with the help of an Autolab potentiostat PGSTAT128N.

3. Results and Discussion

3.1. Physicochemical Characterization of Na-BC

3.1.1. Specific Surface Area

The untreated biochar had a surface area of 100 m²/g and a pzc value of 8.2, and contained about 32% minerals [35]. Treatment with NaOH resulted in several changes to the physicochemical properties of Na-BC. The specific surface area increased to 362 m²/g, while the micropores surface area was 175 m²/g. The N₂ adsorption isotherm and the pore size distribution are presented in Figure 2. It can be seen that Na-BC had a significant amount of micropores, as revealed either from the pore size distribution or from the high value of the adsorbed N₂ amount in low P/Po values. The shape of the isotherm was of the IV type with an H4 hysteresis loop. H4 loops are often found with aggregated crystals of zeolites, some mesoporous zeolites and usually in micro-mesoporous carbons, as in our case [36]. This is also confirmed by the calculation of the micropores surface area with the t-plot method.

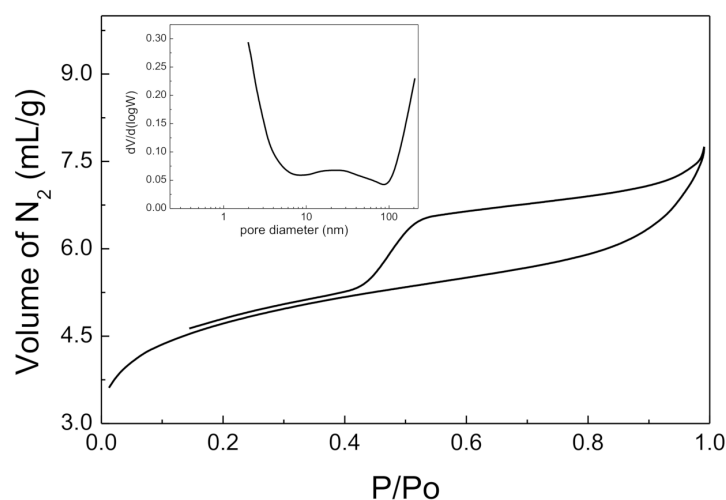


Figure 2. Adsorption-desorption isotherm for the Na-BC sample. Inset: Pore size distribution for the Na-BC sample.

3.1.2. SEM and EDX Analysis

Representative SEM images can be seen in Figure 3. The surface was covered by an inorganic phase, probably oxides or carbonates salts. The capillary tubes of the rootlets were still visible after carbonization and after treatment with NaOH. These pores are in the range of 5 μm and they contribute to the macroporosity of the Na-BC. Conversely, microporosity cannot be detected with SEM images. The EDX analysis of the Na-BC presented in Table 1 denotes that the main components were C and O, with more than 94% in atomic ratio. The surface was enriched with Na as expected due to the NaOH treatment, while P, Ca and K were the main elements detected.

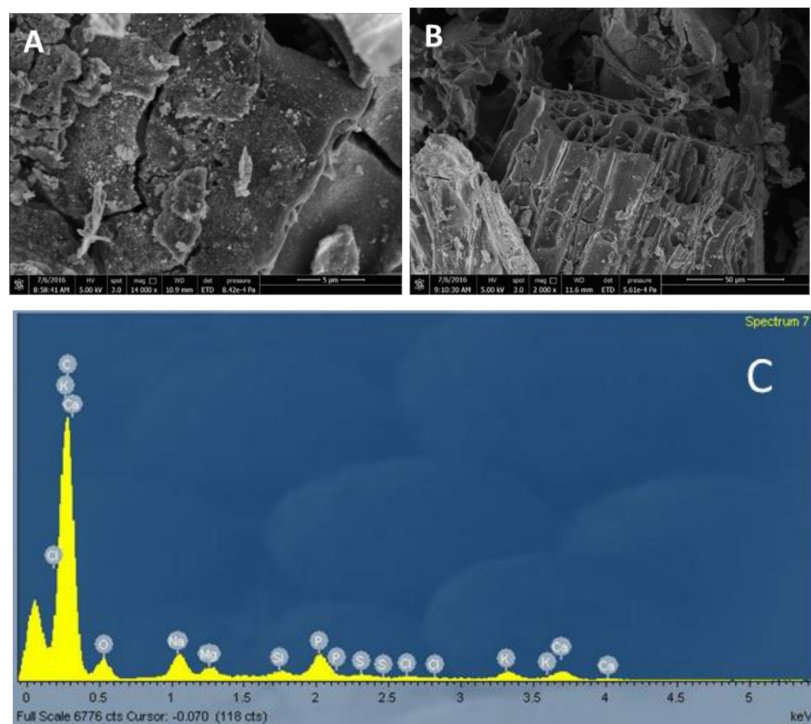


Figure 3. Representative SEM images of Na-BC (A), (B) and EDX analysis (C).

Table 1. % Atomic concentration of elements in Na-BC determined by the EDX analysis.

Element	% Atomic Concentration
C	83.24
O	11.14
Na	1.70
Mg	0.57
Si	0.32
P	1.41
S	0.19
Cl	0.13
K	0.57
Ca	0.72

The main differences of the Na-BC from the starting biochar are related to the Na and O content. The treatment increased Na from non-detectable to 1.70% and O from 10.3 to 11.4 atomic percent. For the other elements, Si, Cl and K gave lower atomic percentages, P and S remained practically the same and Mg and Ca exhibited higher percentages after treatment. This change can be attributed to the partial dissolution of the carbonaceous phase with the minerals on it and the re-precipitation of Mg and Ca due to high basicity.

3.1.3. TGA Analysis

The TGA curve of Na-BC is presented in Figure 4. There is a sharp decrease in the mass of biochar at approximately 400 °C resulting from the burning of the carbon phase in air. The decomposition of the carbon phase is completed at about 500 °C. This temperature range implies that the carbonaceous phase is predominantly cellulose and hemicellulose. This is in agreement with the literature since it is well-known that the NaOH treatment dissolves lignin [37]. After the complete burning of the organic phase, the mass left was approximately 13% of the starting mass. This residue is due to inorganic deposits, especially Na, Ca and K, according to the EDX analysis, either in the form of oxide or carbonates. This value is significantly lower than the 32%, i.e., the quantity of the starting minerals, and its composition was different. Part of the minerals in the starting biochar was dissolved due to the high temperature of the treatment solution, and Na ions were progressively attached to the surface of BC, probably as hydroxides. As a result, the biochar surface was enriched with Na. These minerals exhibit strong interactions with the biochar surface and they were not removed with the addition of water or even with thermal treatment with methanol at 65 °C [32]. Finally, a significant amount of adsorbed water, close to 8%, can be detected from the mass loss in temperature up to 120 °C.

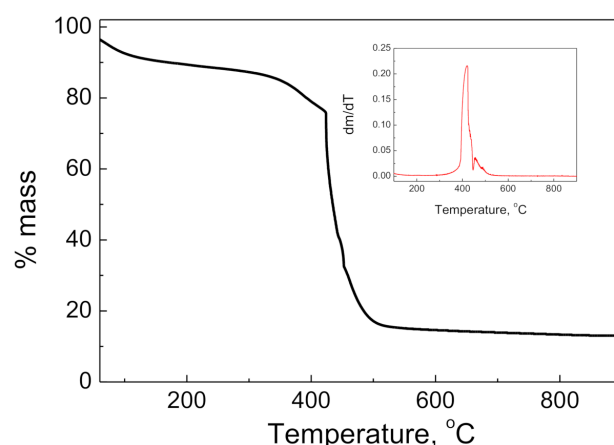


Figure 4. TGA curve of Na-BC. Inset: differential TGA curve.

3.1.4. FTIR Spectroscopy

The FTIR spectrum (Figure 5) of Na-BC clearly shows the presences of oxo groups on the biochar. The peaks at 3400 are due to surface -OH groups and adsorbed H₂O molecules, while the peak at 1033 cm⁻¹ is due to the C-O bonds, pointing out that the -OH groups are in the phenolic structure. This is supported from the peak at 1586 cm⁻¹, which is due to the C=C bond in the aromatic structure. The aromatic phase is poor in H since no peaks corresponding to C-H in aromatic form (wavenumbers higher than 3000 cm⁻¹) were detected. The Na-BC did not have a significant amount of C=O since no characteristic peaks in the region of 1650–1750 cm⁻¹ were detected. Finally, the low intensity of the peaks in the region 1000–1800 cm⁻¹ is characteristic of the heterogeneity of the biochar. [38–40]. The main difference of the Na-BC sample with the starting biochar is the absence of the twin peaks at 2917 and 2836 cm⁻¹ due to the C-H bond in the aliphatic phase. These two peaks are almost not detectable in the FTIR spectrum of the Na-BC. Finally, the treatment with NaOH causes the appearance of a broad band deriving from the overlapping of the different peaks in the area of 1000–1600 cm⁻¹.

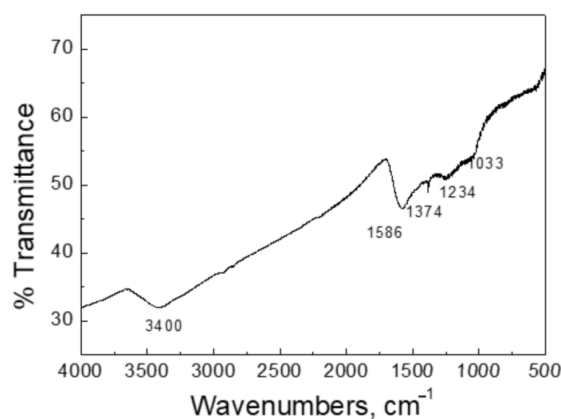


Figure 5. FTIR spectrum of Na-BC.

3.1.5. XRD Analysis

The XRD pattern of Na-BC is shown in Figure 6. There is a broad peak at 25° , which is typical of carbonaceous materials with a less ordered structure due to pyrolysis. In our case this peak was less broad than the peaks usually recorded for biochars. This can be attributed to the removal of lignin, which results in a more homogenous carbonaceous phase. The only peak due to the inorganic phase is the one at 31.4° , which is probably due to halite NaCl [32] although the peak is broader than the sharp peak of halite. The rest of the inorganic phase cannot be detected with the XRD patterns, suggesting that either they are not of high crystallinity or the content of each phase is limited and lower than the detection limit, usually at about 4%.

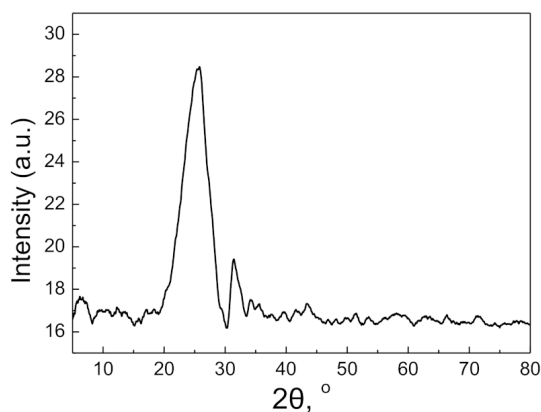


Figure 6. XRD pattern of the Na-BC sample.

3.1.6. Acid-Base Behavior

Acid-base behavior of the Na-BC sample was determined using the potentiometric mass titration method. The titration curves are presented in Figure 7 and denote that the point of zero charge (pzc) of the Na-BC is 9.5. This is the intersection point of the titration curves for the solution and the two suspensions. According to the PMT method, this intersection point corresponds to the pzc value of the solid. The pzc of Na-BC was significantly higher than the pzc of the starting biochar (8.2) pointing out that the NaOH treatment increases the basicity of Na-BC. This can be related to the increase of the Na deposits during treatment as was found by EDX analysis, or even with the dissolution and removal of less basic minerals.

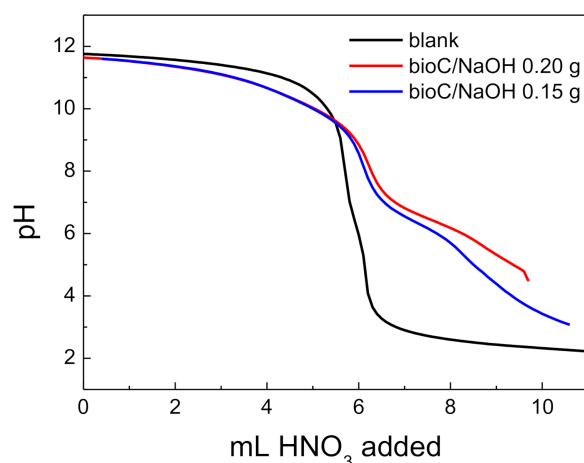


Figure 7. Titration curves for the blank solution and two suspensions of biochar with 0.15 and 0.20 g.

The deviation of the solution titration curve with the suspension curves is more significant after the intersection point. Also, the two curves for the different suspensions exhibit higher differences at pH lower than 7.5, pointing out that the majority of the surface sites on Na-BC are active in this pH region. More details about the amount of H^+ ions consumed by the surface are provided in Figure 8a. An inspection of Figure 8a clearly shows that there was a significant amount of H^+ released in the solution at a pH higher than 10, while the surface consumed H^+ in a pH lower than 8. Surprisingly, there is a pH region between 10 and 8 where the surface does not participate in acid-base reactions. In Figure 8b, the differential curve of the H^+ consumed is presented. It can be seen that there is a broad peak characteristic of the lack of homogeneity of the surface sites of biochar, and a more intense and less broad peak at a pH lower than 7. These peaks represent the surface sites of Na-BC, in the above pH region, which are different from the starting biochar [40].

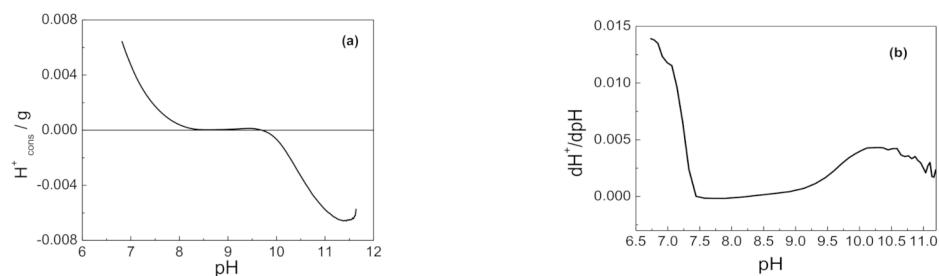


Figure 8. (a) H^+ consumed by the surface as a function of the pH solution; (b) the differential curve of the H^+ consumed with pH.

The above characterization data describe a material with a large active surface created after mild NaOH treatment, which decreased organic content and increased porosity and had a balanced distribution of micro/meso/macro porosity. The material contains substantial active mineral sites and has a surface basic polarity. Such a material, i.e., Na-BC, makes a good candidate for the construction of a supercapacitor.

3.2. Characterization of the Supercapacitor Electrode

Electrodes made by depositing Na-BC on carbon cloth were first characterized by recording their SEM images (Figure 9). As noted, the Na-BC deposition was made by mixing it with a small quantity of carbon black. Carbon black facilitates biochar attachment on carbon cloth but also plays another very important role: because it is highly conductive it assures conductivity channels that transfer electrons to the biochar particles. Indeed, as seen in the image, the biochar particles are surrounded by carbon black nanoparticles, assuring film stability and the facile transfer of charges.

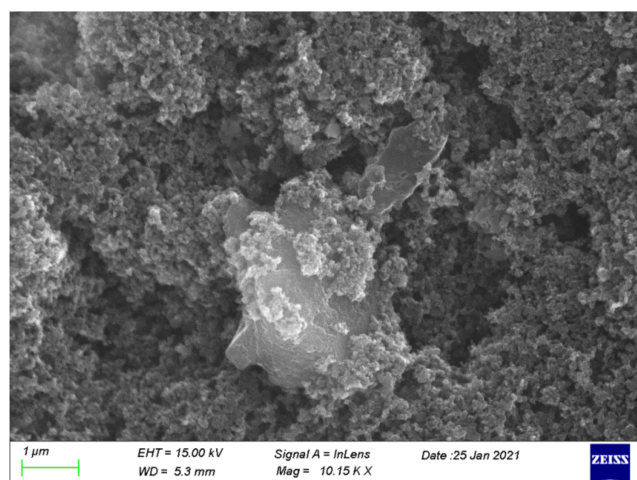


Figure 9. FESEM image of the surface of an Na-BC-carbon black film deposited on carbon cloth.

The specific capacitance of such electrodes was measured by making symmetric cells supporting two identical electrodes and filled with the same electrolyte as that used to run the photocatalytic fuel cell, i.e., 0.5 M aqueous NaOH containing 5% *v/v* ethanol (see Sections 2.4 and 3.3). Figure 10 shows the diagram used to measure the specific capacitance of the Na-BC electrode. The capacitance was calculated by the formula $C = 2 \times I \times t/V$, where I is the (constant) discharge current, V the maximum voltage and t the discharge time. The factor 2 is due to the fact that a symmetric cell corresponds to two capacitors connected in series. The specific capacitance is then obtained by dividing C by the mass of the active material, i.e., 5 mg in our case. Thus the specific capacitance of the presently used Na-BC electrode was calculated to be 156 Fg^{-1} . The same measurement made with a symmetric capacitor composed of electrodes containing only carbon black was very small, i.e., of the order of mFg^{-1} , and it was thus considered negligible. This is a first characteristic that distinguishes the supercapacitor electrode from the counter electrode of the photocatalytic fuel cell (see Figure 1) and differentiates their roles. The specific capacitance of the presently used supercapacitor electrode was smaller but of the same order of magnitude as those recently measured with other biochars [20,25]. However, the advantage carried by Na-BC is the fact that it is produced under mild treatment conditions without tedious or large energy consumption procedures.

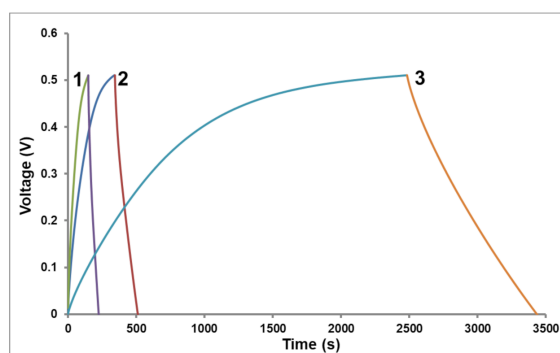


Figure 10. Variation of the voltage of a capacitor made by two identical carbon cloth electrodes each carrying 5 mg of Na-BC under galvanostatic conditions and by applying the charging–discharging procedure. The corresponding current densities in mA cm^{-2} were: (1) 2; (2) 1; and (3) 0.2. The electrolyte was 0.5 M aqueous NaOH containing 5% *v/v* ethanol. The capacitance of each electrode (i.e., each electrochemical double layer) was 156 F g^{-1} .

3.3. Current-Voltage Characteristics of the Photocatalytic Fuel Cell with or without a Supercapacitor Electrode

The current density–voltage characteristics of the photocatalytic fuel cell of Figure 1 were first recorded without the supercapacitor electrode to monitor cell capacities. The diagram in Figure 11A reveals the behavior of a standard photocatalytic fuel cell functioning with a CdS-sensitized titania photoanode and operating with atmospheric oxygen reduction at the cathode electrode. The curve shows a pure photocurrent since the current was practically zero in the dark (see Figure 11B). The short circuit current density (at $V = 0$) was approximately 6 mA cm^{-2} . The cell then produced sufficient photocurrent to charge a supercapacitor, as will be discussed below. It is worth commenting at this point that photocatalytic fuel cells based on mesoporous titania are the only cells that function without external bias. Other popular photocatalysts, such as BiVO_4 , WO_3 and Fe_2O_3 cannot make pure photocatalytic fuel cells since they function only under external bias. This is the reason that CdS-sensitized titania has been used in this work despite the concern that arises from the use of CdS. When such a cell without a supercapacitor electrode was subjected to light chopping at potentiostatic conditions of $V = 0 \text{ V}$, current density quickly reached the maximum photocurrent value under illumination and quickly went to zero in the dark, as seen in Figure 11B. The pattern was recorded during three periodic variations, but remained the same for several hours. It is concluded that in the absence of the supercapacitor, the current is pure photocurrent and it cannot be stored since neither of the two electrodes making the cell provides any storage capacity. This also verifies what was stated above: that the counter electrode, which carries only carbon black, has negligible specific capacitance. Its role is limited to being an air cathode and to carry out oxygen reduction reaction.

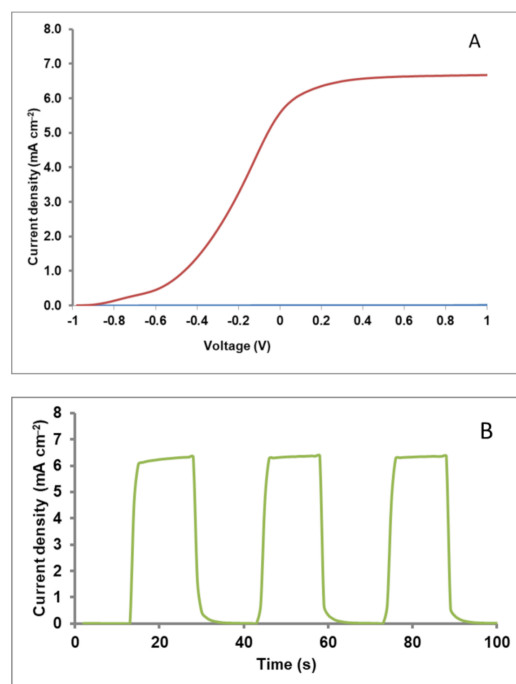


Figure 11. (A) Linear sweep voltammetry with the presently used photocatalytic fuel recorded in a two-electrode configuration (no reference electrode) without a supercapacitor electrode. (B) Potentiostatic variation of the current density at $V = 0 \text{ V}$ by periodic light chopping. The electrolyte was 0.5 M aqueous NaOH containing 5% *v/v* ethanol.

The situation was very different when the supercapacitor electrode was introduced in the cell. Figure 12A shows periodic light chopping in that case. The light was initially turned off and, as expected, the current density was zero. Then the light was turned on. It then took a substantial amount of time to reach the maximum current, which was much lower than in the absence of the supercapacitor electrode. This is expected, since part

of the photogenerated energy is transferred to the supercapacitor. When the light was turned off, the current never became zero in the time range of the measurement, which was now much longer. This pattern was reproduced by turning the light on and off again and continuing in this way for hours. It is obvious that the supercapacitor electrode introduced a charge (and energy) storing functionality to the cell despite the simplicity of the structure and without the need of a sophisticated electrolyte. In order to monitor how long it takes to discharge the capacitor, the light was turned on for a few minutes to make sure that the supercapacitor was charged, and then it was turned off. The current progressively decreased, as shown in Figure 12B, but current flow lasted for more than 10 min under the present conditions. These data show that the introduction of the third electrode loaded with Na-BC makes a storage device; therefore, solar energy conversion and storage was realized with the help of spent malt rootlets biochar.

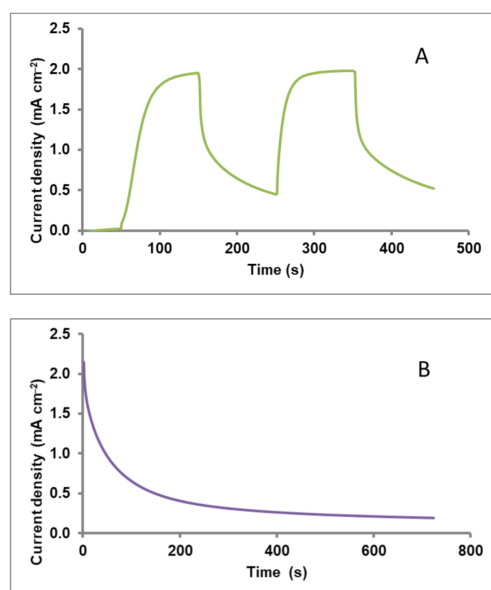


Figure 12. (A) Potentiostatic amperometry at $V = 0$ V by periodic light chopping for the cell with the supercapacitor electrode. (B) Same procedure at a different time scale. The starting point corresponds to a fully charged capacitor.

Finally, it is worth commenting at this point that a combination of biochar-based supercapacitors with photoelectrochemical cells is expected to gain ground because of the simplicity of the device construction and its “green” operation conditions. For example, in a recent publication [20], the energy stored in the supercapacitor was used to sustain photoelectrocatalytic hydrogen production. These systems can be easily upscaled and thus assure applications with several environmental benefits.

4. Conclusions

This work has shown that a supercapacitor electrode can be made by using spent malt rootlets biochar and can be combined with a photocatalytic fuel cell to make a solar energy conversion and storage device. The properties of the biochar dramatically improved by mild treatment in NaOH, which resulted in the extraction of lignin and extensive increase of the specific surface area of the biochar. The combination of a photocatalytic fuel cell with a supercapacitor loaded with biochar, especially with the presently proposed simple configuration comprising one single electrolyte, inexpensive carbon electrodes and photocatalysts, promises to be a new and effective technology for off-grid renewable energy production and storage. In addition, this technology introduces several environmentally beneficial parameters since it proposes the valorization of wastes as energy vectors.

Supplementary Materials: The following are available online at <https://www.mdpi.com/2227-9040/9/3/57/s1>, construction of the photoanode electrode.

Author Contributions: J.V. and P.L. Conceptualization, investigation and manuscript preparation; I.D.M. and V.D. Investigation; D.M. Supervision. All authors have read and agreed to the published version of the manuscript.

Funding: This research received no external funding.

Conflicts of Interest: The authors declare no conflict of interest.

References

1. Qian, L.; Guo, F.; Jia, X.; Zhan, Y.; Zhou, H.; Jiang, X.; Tao, C. Recent development in the synthesis of agricultural and forestry biomass-derived porous carbons for supercapacitor applications: A review. *Ionics* **2020**, *26*, 3705–3723. [[CrossRef](#)]
2. Liu, W.-J.; Jiang, H.; Yu, H.-Q. Development of biochar-based functional materials: Toward a sustainable platform carbon material. *Chem. Rev.* **2015**, *115*, 12251–12285. [[CrossRef](#)]
3. Yuan, J.-H.; Xu, R.-K. The amelioration effects of low temperature biochar generated from nine crop residues on an acidic Ultisol. *Soil Use Manag.* **2011**, *27*, 110–115. [[CrossRef](#)]
4. Cha, J.S.; Park, S.H.; Jung, S.C.; Ryu, C.; Jeon, J.K.; Shin, M.C.; Park, Y.K. Production and utilization of biochar: A review. *Ind. Eng. Chem.* **2016**, *40*, 1–15. [[CrossRef](#)]
5. Inyang, M.; Dickenson, E. The potential role of biochar in the removal of organic and microbial contaminants from potable and reuse water: A review. *Chemosphere* **2015**, *134*, 232–240. [[CrossRef](#)] [[PubMed](#)]
6. Vakros, J. Biochars and their use as transesterification catalysts for biodiesel production: A short review. *Catalysts* **2018**, *8*, 562. [[CrossRef](#)]
7. Shen, B.; Chen, J.; Yue, S.; Li, G. A comparative study of modified cotton biochar and activated carbon based catalysts in low temperature SCR. *Fuel* **2015**, *156*, 47. [[CrossRef](#)]
8. Hasa, B.; Martino, E.; Vakros, J.; Trakakis, G.; Galiotis, C.; Katsaounis, A. Effect of carbon support on the electrocatalytic properties of Pt-Ru catalysts. *Chem. Electron. Chem.* **2019**, *6*, 4970–4979.
9. Mian, M.; Liu, G. Recent progress in biochar-supported photocatalysts: Synthesis, role of biochar, and applications. *RSC Adv.* **2018**, *8*, 14237. [[CrossRef](#)]
10. Tan, X.F.; Liu, Y.G.; Gu, Y.L.; Xu, Y.; Zeng, G.M.; Hu, X.J.; Liu, S.B.; Wang, X.; Liu, S.M.; Li, J. Biochar-based nano-composites for the decontamination of wastewater: A review. *Bioresour. Technol.* **2016**, *212*, 318–333. [[CrossRef](#)]
11. Spanu, D.; Binda, G.; Dossi, C.; Monticelli, D. Biochar as an alternative sustainable platform for sensing applications: A review. *Microchem. J.* **2020**, *159*, 105506. [[CrossRef](#)]
12. Muhammad, H.; Wei, T.; Cao, G.; Yu, S.H.; Ren, X.H.; Jia, H.L.; Saleem, A.; Hua, L.; Guo, J.K.; Li, Y. Study of soil microorganisms modified wheat straw and biochar for reducing cadmium leaching potential and bioavailability. *Chemosphere* **2021**, *273*, 129644. [[CrossRef](#)] [[PubMed](#)]
13. Wang, F.; Ouyang, D.; Zhou, Z.; Page, S.J.; Liu, D.; Zhao, X. Lignocellulosic biomass as sustainable feedstock and materials for power generation and energy storage. *J. Energy Chem.* **2021**, *57*, 247–280. [[CrossRef](#)]
14. Anae, J.; Ahmad, N.; Kumar, V.; Thakur, V.K.; Gutierrez, T.; Yang, X.J.; Cai, C.; Yang, Z.; Coulon, F. Recent advances in biochar engineering for soil contaminated with complex chemical mixtures: Remediation strategies and future perspectives. *Sci. Total Environ.* **2021**, *767*, 144351. [[CrossRef](#)] [[PubMed](#)]
15. Mansoor, S.; Kour, N.; Manhas, S.; Zahid, S.; Wani, O.A.; Sharma, V.; Wijaya, L.; Alyemeni, M.N.; Alsahli, A.A.; El-Serehy, H.A.; et al. Biochar as a tool for effective management of drought and heavy metal toxicity. *Chemosphere* **2021**, *271*, 129458. [[CrossRef](#)]
16. Leng, L.; Xiong, Q.; Yang, L.; Li, H.; Zhou, Y.; Zhang, W.; Jiang, S.; Li, H.; Huang, H. An overview on engineering the surface area and porosity of biochar. *Sci. Total Environ.* **2021**, *763*, 144204. [[CrossRef](#)] [[PubMed](#)]
17. Kamran, U.; Park, S.J. Chemically modified carbonaceous adsorbents for enhanced CO₂ capture: A review. *J. Clean. Prod.* **2021**, *290*, 125776. [[CrossRef](#)]
18. Chi, L.N.T.; Anto, S.; Ahamed, S.T.; Kumar, S.S.; Shanmugam, S.; Samuel, M.S.; Mathimani, T.; Brindhadevi, K.; Pugazhendhi, A. A review on biochar production techniques and biochar based catalyst for biofuel production from algae. *Fuel* **2021**, *287*, 119411. [[CrossRef](#)]
19. Yang, C.S.; Jang, Y.S.; Jeong, H.K. Bamboo-based activated carbon for supercapacitor applications. *Curr. Appl. Phys.* **2014**, *14*, 1616–1620. [[CrossRef](#)]
20. Zhang, J.; Zheng, J.; Yang, W. Green supercapacitor assisted photocatalytic fuel cell system for sustainable hydrogen production. *Chem. Eng. J.* **2021**, *403*, 126368–126377. [[CrossRef](#)]
21. Wang, H.; Wen, J. Biomass porous carbon-based composite for high performance supercapacitor. *Mater. Res. Express* **2020**, *7*, 115601–115612. [[CrossRef](#)]
22. Chen, H.; Hu, H.; Han, F.; Liu, J.; Zhang, Y.; Zheng, Y. CoMoO₄/bamboo charcoal hybrid material for high-energy-density and high cycling stability supercapacitors. *Dalt. Trans.* **2020**, *49*, 10799–10807. [[CrossRef](#)]

23. Cheng, J.; Hu, S.-C.; Sun, G.-T.; Kang, K.; Zhu, M.-Q.; Geng, Z.-C. Comparison of activated carbons prepared by one-step and two-step chemical activation process based on cotton stalk for supercapacitors application. *Energy* **2020**, *215*, 119144–119158. [[CrossRef](#)]
24. Mensah-Darkwa, K.; Zequine, C.; Kahol, P.K.; Gupta, R.K. Supercapacitor energy storage device using biowastes: A sustainable approach to green energy. *Sustainability* **2019**, *11*, 414. [[CrossRef](#)]
25. Andrade, S.T.; Vakros, J.; Mantzavinos, D.; Lianos, P. Biochar obtained by carbonization of spent coffee grounds and its application in the construction of an energy storage device. *Chem. Eng. J. Adv.* **2020**, *4*, 100061. [[CrossRef](#)]
26. Jin, H.; Wang, X.; Shen, Y.; Gu, Z. A high-performance carbon derived from corn stover via microwave and slow pyrolysis for supercapacitors. *J. Anal. Appl. Pyrolysis* **2014**, *110*, 18–23. [[CrossRef](#)]
27. Genovese, M.; Jiang, J.; Lian, K.; Holm, N. High capacitive performance of exfoliated biochar nanosheets from biomass waste corn cob. *J. Mater. Chem. A* **2015**, *3*, 2903–2913. [[CrossRef](#)]
28. Ding, Y.; Wang, T.; Dong, D.; Zhang, Y. Using biochar and coal as the electrode material for supercapacitor applications. *Front. Energy Res.* **2020**, *7*, 159. [[CrossRef](#)]
29. Zhong-Yu, W.; Lei, F.; You-Rong, T.; Wei, W.; Xing-Cai, W.; Jian-Wei, Z. Pomelo peel derived hierarchical porous carbon as electrode materials for high-performance supercapacitor. *Chin. J. Inorg. Chem.* **2018**, *34*, 1249–1260.
30. Subramanian, V.; Luo, C.; Stephan, A.M.; Nahm, K.S.; Thomas, S.; Wei, B. Supercapacitors from activated carbon derived from banana fibers. *J. Phys. Chem. C* **2007**, *111*, 7527–7531. [[CrossRef](#)]
31. Neylon, E.; Arendt, E.K.; Lynch, K.M.; Zannini, E.; Bazzoli, P.; Monin, T.; Sahin, A.W. Rootlets, a malting by-product with great potential. *Fermentation* **2020**, *6*, 117. [[CrossRef](#)]
32. Ntaflou, M.; Vakros, J. Transesterification activity of modified biochars from spent malt rootlets using triacetin. *J. Clean. Prod.* **2020**, *259*, 120931. [[CrossRef](#)]
33. Bourikas, K.; Vakros, J.; Kordulis, C.; Lycourghiotis, A. Potentiometric mass titrations: Experimental and theoretical establishment of a new technique for determining the point of zero charge (PZC) of metal (Hydr)oxides. *J. Phys. Chem. B* **2003**, *107*, 9441–9451. [[CrossRef](#)]
34. Thommes, M.; Kaneko, K.; Neimark, A.V.; Olivier, J.P.; Rodriguez-Reinoso, F.; Rouquerol, J.; Sing, K.S.W. Physisorption of gases, with special reference to the evaluation of surface area and pore size distribution (IUPAC Technical Report). *Pure Appl. Chem.* **2015**, *87*, 1051–1069. [[CrossRef](#)]
35. Martínez, P.M.; Bakker, R.; Harmsen, P.; Gruppen, H.; Kabela, M. Importance of acid or alkali concentration on the removal of xylan and lignin for enzymatic cellulose hydrolysis. *Ind. Crop Prod.* **2015**, *64*, 88–96. [[CrossRef](#)]
36. Tala, W.; Chantara, S. Use of spent coffee ground biochar as ambient PAHs sorbent and novel extraction method for GC-MS analysis. *Environ. Sci. Poll. Res.* **2019**, *26*, 13025–13040. [[CrossRef](#)] [[PubMed](#)]
37. Ballesteros, L.F.; Teixeira, J.A.; Mussatto, S.I. Chemical, functional, and structural properties of spent coffee grounds and coffee silverskin. *Food Bioprocess. Technol.* **2014**, *7*, 3493–3503. [[CrossRef](#)]
38. Magioglou, E.; Frontistis, Z.; Vakros, J.; Manariotis, I.D.; Mantzavinos, D. Activation of persulfate by biochars from valorized olive stones for the degradation of sulfamethoxazole. *Catalysts* **2019**, *9*, 419. [[CrossRef](#)]
39. Bao, N.; Miao, X.; Hu, X.; Zhang, Q.; Jie, X.; Zheng, X. Novel synthesis of plasmonic Ag/AgCl@TiO₂ continuous fibers with enhanced broadband photocatalytic performance. *Catalysts* **2017**, *7*, 117. [[CrossRef](#)]
40. Grilla, E.; Vakros, J.; Konstantinou, I.; Manariotis, I.D.; Mantzavinos, D. Activation of persulfate by biochar from spent malt rootlets for the degradation of trimethoprim in the presence of inorganic ions. *J. Chem. Technol. Biotechnol.* **2020**, *95*, 2348–2358. [[CrossRef](#)]